文章编号：1001-9014(2026)02-0282-06

DOI:10.11972/j.issn.1001-9014.2026.02.011

Millimeter wave imaging of Range Migration Algorithm with adaptive background filtering

CHENG Zhi-Hua[1*], ZHOU Ran[1], WANG Meng[1], YU Tao[1], WANG Yu-Lan[1], YAO Jian-Quan[2]

(1. School of Integrated Circuit Science and Engineering, Tianjin University of Technology, Tianjin 300384, China;
2. Institute of Laser and Opto-electronics, Tianjin University, Tianjin 300191, China)

Abstract: This paper proposes a novel Range Migration Algorithm (RMA) integrated with an adaptive background filtering method specifically designed for near-field millimeter-wave imaging scenarios where targets are in close proximity to background structures. This method simulates the attention distribution mode of the human visual system which is used in Artificial Intelligence (AI) and called the Attention Mechanism. Based on the concept of static clutter filtering, the frequency-domain signals of the scanning aperture are divided into grid cells. Background scattering functions are established by analyzing the motion processes within each cell, and the background interference is linearly filtered out. An analysis of the manifestation of background scattering interference within the algorithm is carried out, and the impact of the grid cell dimension on the imaging quality is investigated. Experimental results show that the proposed method exhibits the capability to enhance the signal-to-noise ratio of both the target and the background. It effectively suppresses the background interference, leading to a more prominent image, meanwhile without imposing the excessive computational load. The method offers a novel solution for improving the performance of millimeter-wave imaging technology in practical applications.

Key words: information processing technology, millimeter-wave imaging, Range Migration Algorithm (RMA), attention mechanism, adaptive background filtering

采用自适应背景滤波的距离徙动算法毫米波成像

程志华[1*], 周 冉[1], 王 猛[1], 于 涛[1], 王玉兰[1], 姚建铨[2]

(1. 天津理工大学 集成电路科学与工程学院,天津 300384;
2. 天津大学 激光与光电子研究所,天津 300191)

摘要:本文针对近场毫米波成像中目标与背景间距很近的情况,提出了一种采用新型自适应背景滤除的距离徙动算法(RMA)。该方法模拟了人工智能(AI)中所采用的人类视觉系统的注意力分配模式,即注意力机制。基于静态杂波滤除的概念,将扫描孔径的频域信号划分为网格单元。通过分析各单元内的运动过程来建立背景散射函数,然后对背景干扰进行线性滤除。对算法内背景散射干扰的表现形式展开了分析,并研究了网格单元尺寸对成像质量的影响。实验结果表明,所提方法具备提高目标和背景信噪比的能力,它能有效抑制背景干扰,使图像更加清晰突出,同时不会产生过高的计算负荷。该方法为提升毫米波成像技术在实际应用中的性能提供了一种新的解决方案。

关 键 词:信息处理技术;毫米波成像;距离徙动算法(RMA);注意力机制;自适应背景滤除

中图分类号:TN015　　**文献标识码**:A

Introduction

Millimeter-wave imaging technology is characterized by its non-destructive nature, non-ionizing properties, and the ability to penetrate non-metallic materials [1-6]. These unique characteristics make it a versatile tool with a wide range of applications, including medical diagnostics [7-8], security screening [5,9-11], and structural inspec-

Received date: 2025-01-13, **revised date**: 2025-03-07　　**收稿日期**:2025-01-13,**修回日期**:2025-03-07

Biography: CHENG Zhi-Hua (1982—), male, Tianjin, lecturer, Ph. D.. Research area involves high-frequency RCS prediction, millimeter-wave radar and microwave technology. E-mail: asakaka1982@163.com

[*] **Corresponding author**: E-mail: asakaka1982@163.com

tion [12].

Several effective near-field imaging algorithms have been developed, such as the Back Projection Algorithm (BPA) [13-15], the Chirp Scaling Algorithm (CSA) [16, 17], and the Range Migration Algorithm (RMA) [18]. Among them, the Range Migration Algorithm (RMA) exhibits higher computational efficiency than the Back Projection Algorithm (BPA) and superior imaging quality compared to the Chirp Scaling Algorithm (CSA). RMA is designed to solve for the target's reflectivity in the frequency domain by approximating the spherical wavefront of the radar signal as a series of planar waves, thereby achieving the high-resolution imaging. Despite its matched filtering characteristics, the performance of RMA is constrained by the frequency modulation rate of the millimeter-wave radar. This limitation poses challenges in distinguishing the target from the background when the spacing is short, particularly in scenarios where certain targets are in proximity to their supporting structures.

For this problem, an accelerated super-resolution range migration algorithm was proposed [19]. The coherent factor (CF) and the enhanced approach for incoherent power can effectively suppress side lobes and background noise. However, this algorithm is mainly applicable to point target imaging. To improve its applicability, the Amplitude Compensation-Range Migration Algorithm (AC-RMA) was proposed [20]. This algorithm compensates for the amplitude of the target signal and enhances the contrast between the target and the background. Nevertheless, it suffers from relatively high time complexity and is susceptible to noise.

To address these issues, the characteristics of the human visual system in focusing on key targets within complex scenes can be emulated [21]. Precisely, the background is effectively mitigated by identifying its characteristic features. In this paper, the background is filtered through an analysis of its electromagnetic properties, geometric configuration, dimensional magnitude, and kinematic characteristics. This approach is founded on the principle of static clutter elimination. Specifically, it divides the frequency-domain signal into grid cells and analyzes the various motion processes during the Synthetic Aperture Radar (SAR) scanning. Through this method, it estimates and filters out the background signal within the grid cells, thereby diminishing the influence of background interference on imaging quality. Compared to the Amplitude Compensation - Range Migration Algorithm (AC-RMA), this algorithm possesses lower time complexity. It can effectively enhance the imaging effect and offers a novel solution for improving the performance of millimeter-wave imaging technology in practical applications.

The structure of this paper is as follows: Section 1 introduces the structure of MIMO-SAR millimeter-wave imaging and provides the main parameters. Section 2 presents an adaptive background filtering algorithm. Section 3 showcases the experimental results to validate the algorithm's effectiveness. Section 4 discusses the influence of grid cell dimensions on images. Finally, the conclusion is presented in Section 5.

1 The structure of the MIMO-SAR imaging system

Near-field imaging of Multiple-Input Multiple-Output Synthetic Aperture Radar (MIMO-SAR) requires a two-dimensional platform. The platform consists of two tracks that are vertical to each other. The MIMO array scans the target along a fixed trajectory, as shown in Fig. 1.

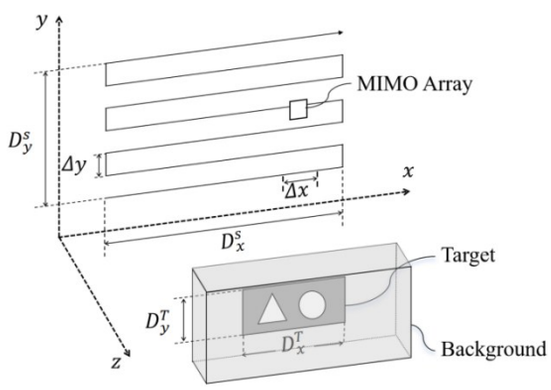

Fig. 1 Basic structure and main parameters of millimeter-wave imaging system
图1 毫米波成像系统的基本结构与主要参数

Define the x-axis and y-axis scanning apertures as:

$$\begin{aligned} D_x^s &= (M_x - 1) \times \Delta x \\ D_y^s &= (M_y - 1) \times \Delta y \end{aligned} \quad , \quad (1)$$

M_x is the number of scanning points of the MIMO array on the x-axis, M_y is the number of scanning points of the MIMO array on the y-axis. Δx and Δy represent the displacements of the array in space.

The frequency modulated continuous wave (FMCW) signal can be described as:

$$s(t) = e^{j2\pi(f_0 t + 0.5Kt^2)}, 0 \leqslant t \leqslant T \quad , \quad (2)$$

where f_0 is the frequency at t=0, K is the frequency slope, and T is the duration of the FMCW.

The received signal can be expressed as:

$$\hat{s}(t) = \sigma m(t - \tau) = \sigma e^{j2\pi(f_0(t-\tau) + 0.5K(t-\tau)^2)} \quad , \quad (3)$$

where τ is the delay time, τ=2R/c, R is the distance between the target and the antenna element, c is the speed of light. σ is the combination of the target reflectivity and the distance between the antenna and the target [9-10,22], is formulated as:

$$\sigma = p/R^2 \quad , \quad (4)$$

where p is the complex scattering coefficient of the target.

The intermediate frequency (beat frequency) signal is expressed as:

$$s_{IF}(t) = \sigma e^{j2\pi(f_0\tau + K\tau t - 0.5K\tau^2)} \quad . \quad (5)$$

The last term of the exponential term is defined as the residual video phase (RVP). The result of the RVP term operation is much smaller than the first two terms, and has no substantial impact on the imaging result. Therefore, the RVP term is ignored. Equation (5) can be rewritten as:

$$s_{\mathrm{IF}}(t)=\sigma e^{j2\pi\tau(f_0+Kt)} \quad . \quad (6)$$

Rewriting to the wave number domain as:

$$s_{\mathrm{IF}}(k)=p\frac{e^{j2kR}}{R^2} \quad . \quad (7)$$

As the virtual element is composed of an equivalent approximation of a transmitter and a receiver, R should be changed to the distance between different virtual units and the target, $R_n=R_u+R_v$, R_u and R_v are respectively the distances from the transmitter and the receiver to the scattering point, as shown in Fig. 2.

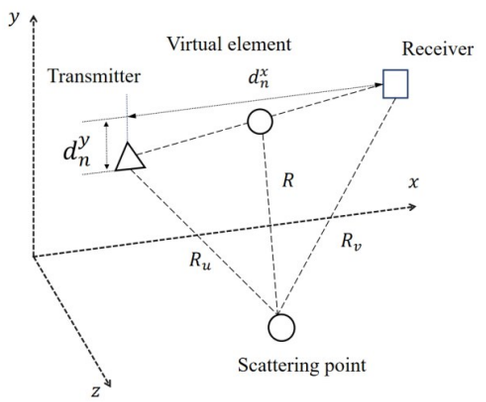

Fig. 2 Spatial positions of transmitter and receiver in MIMO array and equivalent positions of virtual element

图2 MIMO阵列中发射机与接收机的空间位置以及虚拟阵元的等效位置

The coordinate of the virtual element is equivalent to $(x,y,0)$:

$$R_n\approx 2R+\frac{\left(d_n^x\right)^2+\left(d_n^y\right)^2}{4R} \quad . \quad (8)$$

The frequency response of the virtual element is:

$$s_{\mathrm{IF}}(k)=p\frac{e^{j2ke^{j2kR}}e^{j\varphi_n(k)}}{R_uR_v} \quad , \quad (9)$$

where

$$\varphi_n(k)=k\frac{\left(d_n^{x^2}\right)+\left(d_n^y\right)^2}{4z_0} \quad . \quad (10)$$

2 Adaptive background filtering algorithm

To reduce the computational complexity, only process the frequency domain signals within the target range gate. Suppose that the reflectivity of the target in space is $p(x',y')$, then the expression of Eq. (9) on the two-dimensional plane is

$$\begin{aligned}S_{\mathrm{IF}}^{\omega}(x,y)&=\int\int s_{\mathrm{IF}}^{\omega}(x',y')\mathrm{d}x'\mathrm{d}y'\\&=\iint p(x',y')\frac{e^{j2kR}}{R_uR_v}\mathrm{d}x'\mathrm{d}y' \quad , \quad (11)\end{aligned}$$

where ω is the corresponding range gate frequency.

The amplitude term $\frac{1}{R_uR_v}$ can be rewritten as $\frac{1}{z_0R}$. The key to improving imaging quality lies in the processing of the phase term.

Express the spherical wave as the superposition of plane waves:

$$\frac{e^{j2kR}}{R}=\frac{j}{2\pi}\iint\frac{e^{j\left(k_x(x-x')+k_y(y-y')+k_zz_0\right)}}{k_z}\mathrm{d}k_x\mathrm{d}k_y \quad , \quad (12)$$

where

$$\begin{aligned}k_z&=\sqrt{4k^2-k_x^2-k_y^2}\\k_x&=\frac{2\pi}{\Delta x},k_y=\frac{2\pi}{\Delta y} \quad , \quad (13)\end{aligned}$$

k_x, k_y and k_z are the components of the wave number in the x, y, and z axes. Substitute Eq. (12) into Eq. (11), and ignore the constant term:

$$\begin{aligned}S_{\mathrm{IF}}^{\omega}(x,y)=\frac{j}{2\pi}\iint\left(\iint p(x',y')e^{-j\left(k_xx'+k_yy'\right)}\mathrm{d}x'\mathrm{d}y'\right)\\\frac{e^{jk_zz_0}}{k_z}e^{j\left(k_xx+k_yy\right)}\mathrm{d}k_x\mathrm{d}k_y \quad . \quad (14)\end{aligned}$$

The scanning aperture effectively covers the target aperture, x', y' and x, y are overlapping, x', y' can be directly rewritten as x, y:

$$p(x,y)=\mathrm{IFT}\left(S_{\mathrm{IF}}^{\omega}\left(k_x,k_y\right)k_ze^{-jk_zz_0}\right) \quad . \quad (15)$$

The reflectivity in Eq. (15) is actually composed of the target reflectivity and the background reflectivity. In the short spacing between target and background cases, the target signal will be interfered or even submerged by the background scattering, resulting in a poor imaging effect. In this paper, the idea of filtering out static clutter is adopted to solve this problem.

The process of a dynamic array scanning a static target is approximated to a static array scanning a dynamic target, similar to the situation of inverse synthetic aperture radar (ISAR). In this approximate state, the background is dynamic relative to the array, but it has a much larger area than the target and its material is uniform. Take the background as stationary and estimate the background scattering by utilizing the frequency domain signals of different motion processes.

Divide different motion processes into grids in a plane. Each grid cell contains N_x horizontal pixels and N_y vertical pixels. To ensure the image quality, the dimension of the grid cells depends on the dimension of the target. When performing imaging reconstruction for unknown targets, the geometric dimensions of the target serve as prior knowledge. The construction of a ratio factor establishes a quantitative relationship between target features and grid units, thereby enabling the derivation of optimal grid parameters. The mathematical derivations and implementation procedures of this methodology are comprehensively elaborated in Section 4. The expression for the static clutter estimation of the m-th grid cell is:

$$s_{\mathrm{Back}}^{m}(x',y')=\frac{1}{N_xN_y}\sum_{(m-1)N_x+1}^{mN_x}\sum_{(m-1)N_y+1}^{mN_y}s_{\mathrm{IF}}^{\omega}(x',y') \quad . \quad (16)$$

The number of grid cells is $\frac{M_xM_y}{N_xN_y}$, $m\in[1,\frac{M_xM_y}{N_xN_y}]$. After filtering out the background, the signal in the grid cell is:

$$\overline{s_{\mathrm{IF}}^{\omega}}(x',y')=s_{\mathrm{IF}}^{\omega}(x',y')-s_{\mathrm{Back}}^{m}(x',y') \quad . \quad (17)$$

This method keeps the background scattering within an acceptable range and preserves the target details.

Grid division effectively mitigates blurring at target edges, since the frequency-domain signals between grid units remain relatively independent and are not subject to interference from adjacent grids, thereby granting the frequency-domain signals at target edge adaptive properties.

The time complexity of this algorithm is $O(\frac{N^2}{N_x N_y})$, which is inversely proportional to the dimension of the grid cell. Time complexity of RMA is $O(N^2)$, after combining with the adaptive background filtering algorithm, the time complexity is $O(N^2)+O(\frac{N^2}{N_x N_y})$. It imposes no excessive computational load and proves advantageous for real-time imaging implementation. The program flow chart is shown in Fig. 3.

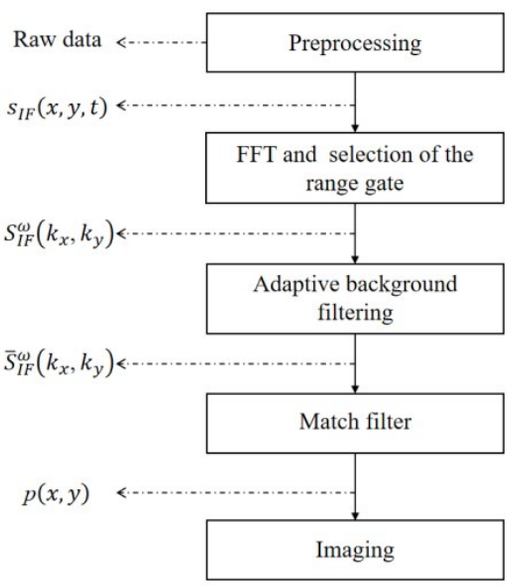

Fig. 3 The flow chart of the RMA with adaptive background filtering
图3 采用自适应背景滤波的RMA流程图

3 Experiments

The experimental configuration is listed in Table 1. Figure 4 compares the imaging results among the adaptive background-filtered imaging, the AC-RMA imaging, and the original RMA imaging under identical contrast conditions. The results demonstrate that the adaptive background filtering enhances the image and effectively suppresses the background noise while more effectively filtering out the background compared with AC-RMA.

Figure 5 displays horizontal profile comparisons of images generated by different algorithms. Blue boxes in the figure mark target regions and red boxes indicate background areas. For Target 1 imaging analysis, the green box identifies artifact signals. While artifacts may originate from various sources, the specific artifact observed here is dominantly caused by the multipath propagation through the enclosed cardboard structure. Note that the artifact analysis is not the primary objective of this study. These annotations are provided solely for the visual reference; artifact generation mechanisms and suppression techniques lie outside the scope of this work. In both original RMA and AC-RMA imaging results, the target remains nearly obscured by the background. The adaptive background-filtered imaging significantly enhances the target signal while suppressing the background interference.

Table 1 Experimental and radar parameters
表1 实验及雷达配置

Parameter	Value
Sensor-to-target distance (mm)	570
Scanning aperture (mm)	400×400
Scanning step (mm)	$\Delta x = 1, \Delta y = 2$
Frequency band (GHz)	77-81
Frequency slope (GHz)	70×10^3
Sampling frequency (MHz)	5
Sampling number	256

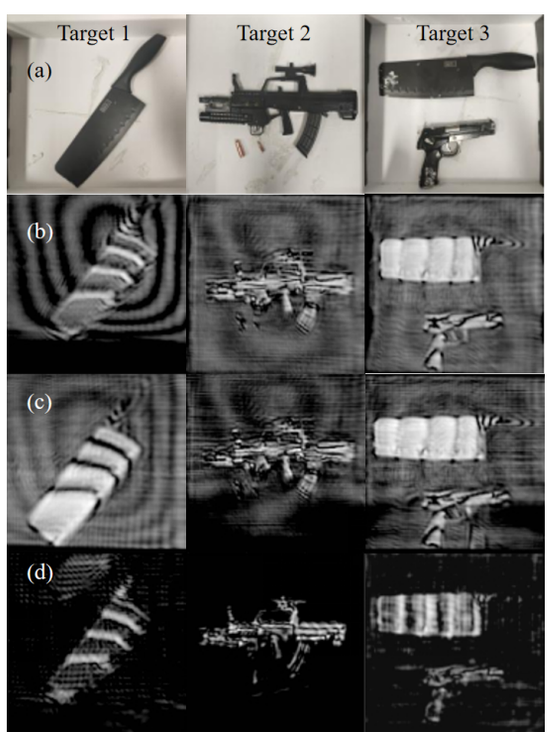

Fig. 4 Imaging effects of different algorithms: (a) imaging target; (b) imaging of RMA; (c) imaging of AC-RMA; (d) imaging of RMA with adaptive background filtering
图4 不同算法的成像效果:(a) 成像目标;(b) RMA成像;(c) AC-RMA成像;(d) 采用自适应背景滤波的RMA成像

The experiment utilized a computer equipped with an Intel (R) Core (TM) i7 - 8750H CPU and 16.0 GB of onboard random-access memory (RAM), with approximately 15.9 GB available for use. The operating system was Windows 10 Professional. As can be seen from the program execution time data in Table 2, under the same operating environment, the execution duration of the improved algorithm proposed in this paper is similar to that of the original RMA algorithm.

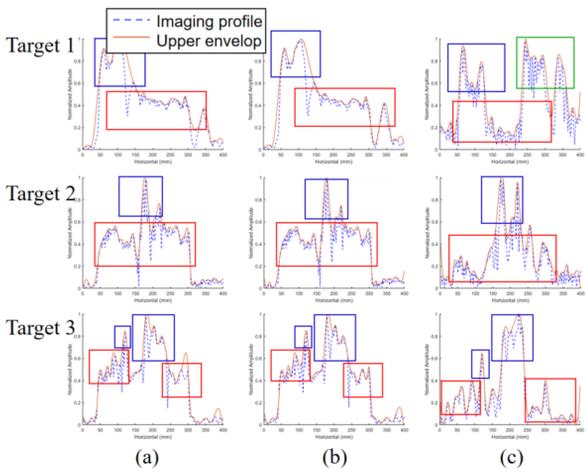

Fig. 5 Imaging profiles of different algorithms: (a) imaging profiles of RMA; (b) imaging profiles of AC-RMA; (c) imaging profiles of RMA with adaptive background filtering
图5 不同算法的成像剖面:(a) RMA成像剖面;(b) AC-RMA成像剖面;(c) 采用自适应背景滤波的RMA成像剖面

Table 2 Program execution time (s)
表2 程序执行时间(s)

	RMA	RMA with Adaptive Background Filtering
Target 1	5.850	6.125
Target 2	5.737	5.839
Target 3	5.809	5.859

4 Discussion

The dimension of the grid cell is contingent upon the dimension of the target. Generally, the smaller the grid cell, the more effective the filtering. However, excessive filtering may lead to over-processing of the image. A judicious grid dimension should enclose the edges of the target without over-processing the target signal. In this section, experiments were conducted regarding the dimension of grid cells, and thereafter, conclusions were drawn.

The processing degree of the signal is measured by the ratio factor (RF):

$$\mathrm{RF} = \log\left(\left\| S_{\mathrm{in}} \right\|_2^2 \Big/ \left\| S_{\mathrm{out}} \right\|_2^2\right) = \log\left(\left\| s_{\mathrm{IF}}^{\omega} \right\|_2^2 \Big/ \left\| \overline{s_{\mathrm{IF}}^{\omega}} \right\|_2^2\right). \quad (18)$$

In Fig. 6, the RF decreases as the grid cell dimension increases. This occurs because the average values within the grid cells tend to become more similar, effectively appearing as a constant within the context of the algorithm.

Determining a reasonable grid cell dimension requires considering both signal processing and satisfactory imaging results. For comparison purposes, reference values with relatively high processing degrees in Fig. 6 are selected, namely 2 mm, 6 mm, 8 mm, 16 mm, 52 mm, and 56 mm, respectively. When the grid cell dimension is set to 2 mm×2 mm, the excessive processing phenomena occur, thereby rendering it eligible for exclusion from further consideration. Figure 7 illustrates that, under comparable processing degrees, a smaller grid cell size yields a better imaging effect. A smaller grid cell is more capable of accurately representing the scattering level within a given region.

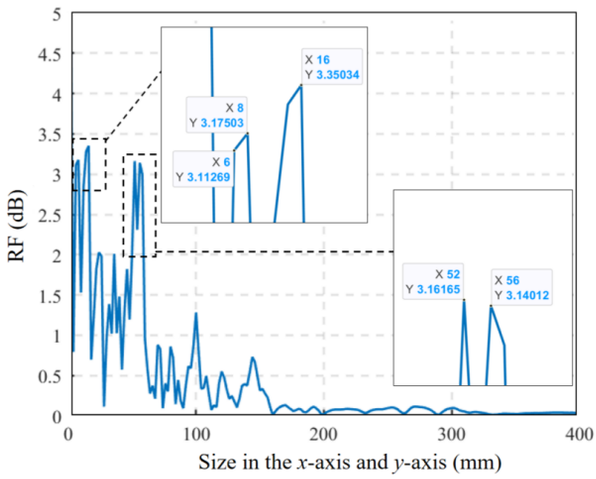

Fig. 6 RF with different grid cell dimensions
图6 不同网格单元尺寸下的RF

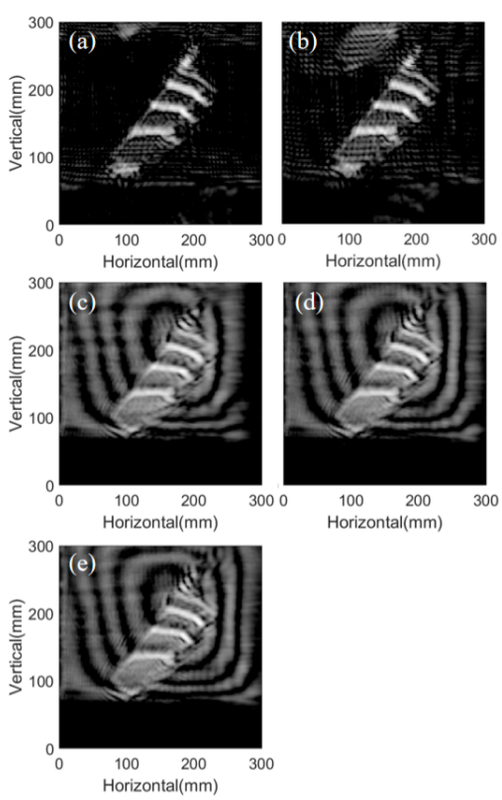

Fig. 7 Imaging effects under different grid dimensions: (a) image with grid cell dimension of 6 mm×6 mm; (b) image with grid cell dimension of 8 mm×8 mm; (c) image with grid cell dimension of 16 mm×16 mm; (d) image with grid cell dimension of 52 mm×52 mm; (e) image with grid cell dimension of 56 mm×56 mm
图7 不同网格尺寸下的成像效果:(a)网格单元尺寸为6 mm×6 mm的图像;(b)网格单元尺寸为8 mm×8 mm的图像;(c)网格单元尺寸为16 mm×16 mm的图像;(d)网格单元尺寸为52 mm×52 mm的图像;(e)网格单元尺寸为56 mm×56 mm的图像

5 Conclusion

This paper proposes an attention mechanism-inspired adaptive background filtering strategy within the RMA. In the frequency domain, the signals are partitioned into grid cells within the planar domain, and the mean values of these grid cells are computed to achieve the background filtering. This algorithm effectively suppresses the background reflection signals within the aperture. The experimental results validate that it can enhance the signal-to-noise ratio of both the target and the background, while maintaining a relatively low level of time complexity. Through the discussion on the impact of grid cell dimension on the image, it is concluded that a reduction in grid cell dimension is conducive to the improvement of image quality under a relatively high level of signal processing. This algorithm proffers a solution for augmenting the imaging quality in situations where the distance between the target and the background is relatively short.

The innovative integration of this algorithm with the attention mechanism is feasible. The attention allocation mechanism is emulated to precisely focus on the target area and suppress the background noise interference in complex environments. The algorithm enhances the system′s capacity for target object acquisition in security inspections and precisely identifies lesion areas in medical diagnoses. This paper provides a feasible technical approach for optimizing the performance of the Radar Imaging System.

References

[1] Sheen D L, McMakin D L, Hall T E. Near-field three-dimensional radar imaging techniques and applications[J]. Appl. Opt., 2010, 49(19): E83-E93.
[2] Cooper K B, Dengler R J, Llombart N, et al. THz imaging radar for standoff personnel screening[J]. IEEE Trans. Terahertz Sci. Technol., 2011, 1(1): 169-182.
[3] Cooper K B. Penetrating 3-D imaging at 4- and 25-m range using a submillimeter-wave radar[J]. IEEE Trans. Microw. Theory Techn., 2008, 56(12): 2771-2778.
[4] Sheen D L, McMakin D L, Collins H, et al. Near-field millimeter-wave imaging for weapons detection[C]. Proc. SPIE. 1993, 1824: 223-233.
[5] Sheen D L, McMakin D L, Hall T E. Three-dimensional millimeter-wave imaging for concealed weapon detection[J]. IEEE Trans. Microw. Theory Techn., 2001, 49(9): 1581-1592.
[6] Lin B, Li C, Ji Y C, et al. Efficient scaling techniques for 2-D sparse MIMO array far-field imaging[J]. IEEE Sens. J., 2024, 24(8): 12604-12615.
[7] Liu C, Afsar M N, Korolev K A. Millimeter wave dielectric spectroscopy and breast cancer imaging[C]. 2012 7th European Microwave Integrated Circuit Conference, Amsterdam, 2012.
[8] Gao Y, Zoughi R. Millimeter wave reflectometry and imaging for noninvasive diagnosis of skin burn injuries[J]. IEEE Trans. Instrum. Meas., 2017, 66(1): 77-84.
[9] Zhuge X D, Yarovoy A G. Three-dimensional near-field MIMO array imaging using range migration techniques[J]. IEEE Trans. Image Process., 2012, 21(6): 3026-3033.
[10] Yanik M E, Torlak M. Near-field 2-D SAR imaging by millimeter-wave radar for concealed item detection[C]. 2019 IEEE Radio and Wireless Symposium (RWS), 2019: 1-4.
[11] Gao J K, Qin Y L, Deng B, et al. Novel efficient 3D short-range imaging algorithms for a scanning 1D-MIMO array[J]. IEEE Trans. Image Process., 2018, 27(7): 3631-3643.
[12] Kharkovsky S, Case J T, Zoughi R, et al. Millimeter wave detection of localized anomalies in the space shuttle external fuel tank insulating foam and acreage heat tiles[C]. 2005 IEEE Instrumentation and Measurement Technology Conference Proceedings, 2005: 1527-1530.
[13] Smith J W, Torlak M. Efficient 3-D near-field MIMO-SAR imaging for irregular scanning geometries[J]. IEEE Access, 2022, 10: 10283-10294.
[14] Kidera S, Sakamoto T, Sato T. Accurate UWB radar three-dimensional imaging algorithm for a complex boundary without range point connections[J]. IEEE Trans. Geosci. Remote Sens., 2010, 48(4): 1993-2004.
[15] Sasaki Y, Shang F, Kidera S, et al. Three-dimensional imaging method incorporating range points migration and Doppler velocity estimation for UWB millimeter-wave radar[J]. IEEE Geosci. Remote Sens. Lett., 2017, 14(1): 122-126.
[16] Zhang W R, Ji Y C, Shao W Y, et al. A fast 3-D chirp scaling imaging technique for millimeter-wave near-field imaging[J]. IEEE Trans. Microw. Theory Techn., 2023, 71(2): 827-841.
[17] Wei Y M, Qiu X L, Xi L, et al. An efficient range scaling algorithm for MIMO-SAR 3-D imaging[J]. IEEE Trans. Microw. Theory Techn., 2024, 72(8): 4945-4959.
[18] Zhu R Q, Zhou J X, Jiang G, et al. Range migration algorithm for near-field MIMO-SAR imaging[J]. IEEE Geosci. Remote Sens. Lett., 2017, 14(12): 2280-2284.
[19] Manzoor Z, Qaseer M T A, Donnell K M. A comprehensive bi-static amplitude compensated range migration algorithm (AC-RMA)[J]. IEEE Trans. Image Process., 2021, 30: 7038-7049.
[20] Guo Q J, Liang J, Chang T Y, et al. Millimeter-wave imaging with accelerated super-resolution range migration algorithm[J]. IEEE Trans. Microw. Theory Techn., 2019, 67(11): 4610-4621.
[21] Vaswani A, Shazeer N, Parmar N, et al. Attention is all you need[C]. Proc. Adv. Neural Inf. Process. Syst., 2017: 5998-6008.
[22] Qiao L B, Wang Y X, Zhao Z R, et al. Exact reconstruction for near-field three-dimensional planar millimeter-wave holographic imaging[J]. Journal of Infrared Millimeter & Terahertz Waves, 2015, 36(12): 1221-1236.